Discovery of novel tumor suppressors from CRISPR screens reveals lipid-sensitive subtype of AML

W. Frank Lenoir[1,2], Micaela Morgado[2], Peter C DeWeirdt[3], Megan McLaughlin[1,2], Audrey L Griffith[3], Annabel K Sangree[3], Marissa N Feeley[3], Eiru Kim[2], Medina Colic[1,2], Merve Dede[1,2], John G Doench[3], Traver Hart[2,4,*]

1 - The University of Texas MD Anderson Cancer Center UTHealth Graduate School of Biomedical Sciences; The University of Texas MD Anderson Cancer Center, Houston, TX

2 - Department of Bioinformatics and Computational Biology, The University of Texas MD Anderson Cancer Center, Houston, TX, USA

3 - Genetic Perturbation Platform, Broad Institute of MIT and Harvard, Cambridge, MA, USA

4 - Department of Cancer Biology, The University of Texas MD Anderson Cancer Center, Houston, TX, USA

* - Corresponding author: traver@hart-lab.org

Abstract

CRISPR knockout screens in hundreds of cancer cell lines have revealed a substantial number of context-specific essential genes that, when associated with a biomarker such as lineage or oncogenic mutation, offer candidate tumor-specific vulnerabilities for targeted therapies or novel drug development. Data-driven analysis of knockout fitness screens also yields many other functionally coherent modules that show emergent essentiality or, in some cases, the opposite phenotype of faster proliferation. We develop a systematic approach to classify these suppressors of proliferation, which are highly enriched for tumor suppressor genes, and define a network of 103 genes in 22 discrete modules. One surprising module contains several elements of the glycerolipid biosynthesis pathway and operates exclusively in a subset of AML lines, which we call Fatty Acid Synthesis/Tumor Suppressor (FASTS) cells. Genetic and biochemical validation indicates that these cells operate at the limit of their carrying capacity for saturated fatty acids. Overexpression of saturated acyltransferase *GPAT4* or its regulator *CHP1* confers a survival advantage in an age-matched cohort of AML patients, indicating the in vitro phenotype reflects a clinically relevant subtype, and suggesting a previously unrecognized risk in clinical trials for fatty acid synthesis pathway inhibitors.

Introduction

Gene knockouts are a fundamental weapon in the geneticist's arsenal, and the discovery of CRISPR-based genome editing[1] and its adaptation to gene knockout screens has revolutionized mammalian functional genomics and cancer targeting[2–8]. Hundreds of CRISPR/Cas9 knockout screens in cancer cell lines have revealed background-specific genetic vulnerabilities[9–13], providing guidance for tumor-specific therapies and the development of novel targeted agents. Although lineage and mutation state are powerful predictors of context-dependent gene essentiality, variation in cell growth medium and environment can also drive differences in cell state, particularly among metabolic genes[14,15], and targeted screening can reveal the genetic determinants of metabolic pathway buffering[16,17].

The presence and composition of metabolic and other functional modules in the cell can also be inferred by integrative analysis of large numbers of screens. Correlated gene knockout fitness profiles, measured across hundreds of screens, have been used to infer gene function and the modular architecture of the human cell[18–21]. Data-driven analysis of correlation networks reveals clusters of functionally related genes whose emergent essentiality in specific cell backgrounds is often unexplained by the underlying lineage or mutational landscape[21]. Interestingly, in a recent study of paralogs whose functional buffering renders them systematically invisible to monogenic CRISPR knockout screens[22,23], it was shown that the majority of context-dependent essential genes are constitutively expressed in cell lines[23]. Collectively these observations suggest that there is much unexplained variation in the genetic architecture, and emergent vulnerability, of tumor cells.

Building human functional interaction networks from correlated gene knockout fitness profiles in cancer cells is analogous to the yeast functional interaction networks from correlated genetic interaction profiles[24–27]. The fundamental difference between the two approaches is that, in yeast, a massive screening of pairwise gene knockouts in a single yeast strain was conducted in order to measure genetic interaction - a dual knockout phenotype more or less severe than that expected by the combination of the two genes independently. In coessentiality networks, CRISPR-mediated single gene knockouts are conducted across a panel of cell lines that sample the diversity of cancer genotypes and lineages. Digenic perturbations in human cells, a more faithful replication of the yeast approach, are possible with Cas9 and its variants, but library

construction, sequencing, and positional biases can be problematic[16,28–34]. Recently, we showed that an engineered variant of the Cas12a endonuclease, enCas12a[35], could efficiently perform multiplex gene knockouts[34], and we demonstrated its effectiveness in assaying synthetic lethality between targeted paralogs[23]. These developments in principle enable researchers to measure how biological networks vary across backgrounds, a powerful approach for deciphering complex biology[24,36,37].

CRISPR perturbations in human cells can result in loss of function alleles that increase as well as decrease *in vitro* proliferation rates, an extreme rarity in yeast knockouts. These fast-growers can complicate predictions of genetic interaction[29] and confound chemoresistance screens[38]. However, there is no broadly accepted method of classifying these genes from CRISPR screens. Here we describe the development of a method to systematically identify genes whose knockout provides a proliferation advantage *in vitro*. We observe that genes which confer proliferation advantage are typically tumor suppressor genes, and show the same trends of co-occurrence and functional coherence as the pathways and complexes identified in network analyses of context-dependent essential genes. Moreover, we discover a novel module that includes several components of the glycerolipid biosynthesis pathway that slows cell proliferation in a subset of AML cell lines, and we show a rewired genetic interaction network using enCas12a multiplex screening, with strong genetic interactions corroborated by clinical survival data. A putative tumor-suppressive role for glycerolipid biosynthesis is surprising since this process is thought to be required to generate biomass for tumor cell growth, and may represent an unanticipated risk factor for pathway inhibitors currently in clinical trials[39,40].

Results

Identifying Proliferation Suppressor Signatures

We previously observed genes whose knockout leads to overrepresentation in pooled library knockout screens. These genes, which we term proliferation suppressor (PS) genes, exhibit positive selection in fitness screens, a phenotype opposite that of essential genes. As expected, many PS genes are known tumor suppressor genes; for example, *TP53* and related pathway genes *CDKN1A*, *CHEK2*, and *TP53BP1* show positive selection in select cell lines (**Figure 1a**). Detection of these genes as outliers is robust to the choice of CRISPR analytical method, as we tested BAGEL2, CERES, JACKS, and mean log fold change (LFC) (**Supplementary Figure 1a-**

d). Unlike core-essential genes, PS genes are highly background-specific: *TP53* knockout shows positive LFC only in cell lines with wild-type *TP53* (**Figure 1b**), and *PTEN* knockout shows the PS phenotype only in $PTEN^{wt}$ backgrounds (**Figure 1c**). These observations are consistent with the role of tumor suppressor genes (TSG) in cell lines: in wildtype cells, TSG knockout increases the proliferation rate in cell culture, but when cell lines are derived from tumors where the TSG is already lost, gene knockout has no effect. TSG are therefore context-specific PS genes, but it is not necessarily the case that genes with a PS phenotype *in vitro* act as TSG *in vivo;* PS genes are at best putative TSG in the absence of confirmatory data from tumor profiling.

Though detection of known PS genes is possible using existing informatics pipelines, several factors complicate a robust detection of these genes. There is no accepted threshold for any algorithm we considered to detect PS genes, since all were optimized to classify essential genes. A related second issue is that cell line screens show a wide range of variance in LFC distributions, making robust outlier detection challenging (**Supplementary Figure 1e**). Third, the signatures are strongly background-dependent, as demonstrated by PTEN and TP53. Finally, there is no consistent expectation for whether or how many putative tumor suppressor genes are present in a given cell line.

To address this gap, we developed a method to detect proliferation suppressor genes based on the normalized mean LFC of gRNA targeting a gene. To generate a null distribution, we label-shuffled guide-level LFC values for each screen, calculated gene-level mean fold change, and repeated this shuffling 1,000 times (**Figure 1d**). We used the mean and standard deviation of this randomized distribution of gene-level mean fold changes to calculate a Z-score for raw gene-level mean fold change for each cell line. This approach normalizes variance (**Supplementary Figure 1e-f**) across LFC distributions in different cell lines.

To evaluate the effectiveness of this shuffled Z-score approach, we used COSMIC[41,42] tumor suppressor genes as a positive reference set, and we combined COSMIC-defined oncogenes (removing dual-annotated tumor suppressors) with our previously-specified set of nonessential genes as a negative reference set[8,43]. Since there is no consistent expectation for the presence of PS genes across cell lines, we analyzed each of the 563 cell lines from the Avana 2019q2 data release independently[10,44,45], calculating gene-level scores on each cell line individually and then combining all scores into a master list of 563 x 17k = 9.8 million gene-cell line observations

(**Supplementary Table 1**). Moreover, since there is also no expectation that all COSMIC TSG would be detected cumulatively across all cell lines, and similarly no expectation that any subset of known TSG would be detected in all cell lines, we judged that traditional recall metrics (e.g. percentage of the reference set recovered) were inappropriate. We therefore defined recall as the total number of TSG-cell line observations. Using this evaluation scheme, the shuffled Z-score approach outperforms comparable methods by a substantial margin, identifying more than 500 PS-cell line instances at a 10% false discovery rate (FDR) (**Figure 1e**). This is roughly 50% more than the closest alternatives, JACKS[46] and a nonparametric rank-based approach. BAGEL[47,48], a supervised classifier of essential genes, performed worst at detecting PS genes, and the raw mean LFC approach also fared poorly, highlighting the need for variance normalization across experiments. We applied this 10% FDR threshold for all subsequent analyses.

Common tumor suppressor genes PTEN and TP53 were observed in ~15% of cell lines (**Figure 1f**), with other well-known tumor suppressor genes appearing less frequently. Among 288 COSMIC TSGs for which we have fitness profiles (representing 1.65% of all 17k genes), we find that 58 (20.1%) of these genes occur as proliferation suppressors at least once (**Supplementary Table 2**), and make up 16.6% of total proliferation suppressor calls (**Supplementary Figure 2a-b**), a 10-fold enrichment. All of the known TSG hits come from just 249 of the 563 cell lines (49.7%) in which proliferation suppressor hit calls were identified (**Figure 1g**), yet we did not observe a bias toward particular tissues: in every lineage, most cell lines carried at least one PS gene (**Supplementary Figure 1g**).

To further validate our approach, we compared the set of TSGs in our PS hits to other molecular profiling data. When identified as a proliferation suppressor, 63% of the 58 TSGs demonstrate higher mRNA expression relative to backgrounds where the same TSG is not a proliferation suppressor (**Supplementary Figure 2c** and **Supplementary Table 2**). Similarly, 84.5% of the 58 TSGs, when identified as a proliferation suppressor, demonstrate lower rates of nonsilent mutations compared to backgrounds where the TSG is not a hit (**Supplementary Figure 2d & Supplementary Table 2**). Together, these observations confirm the reliability of our method to detect genes whose knockout results in faster cell proliferation, and that, analogous to essential genes, these genes must be expressed and must not harbor a loss-of-function mutation in order to elicit this phenotype.

We attempted to corroborate our findings using a second CRISPR dataset of 342 cell line screens from Behan *et al.*[13], including >150 screens in the same cell lines as in the Avana data. However, these screens were conducted over a shorter timeframe than the Avana screens (14 vs. 21 days), giving less time for both positive and negative selection signals to appear. The fitness enhancement introduced by PS gene knockout, relatively weak compared to severe defects from essential gene knockout, often precludes detection in a shorter experiment. In the example F5 cell line (**Figure 1a**), a 2.5-fold change over a 21-day time course corresponds to a fitness increase of only ~12% for rapidly growing cells, or a doubling time decrease from 24 to 21 hours. In a 14-day experiment, this increased proliferation rate would result in an observed log fold change of only ~1.7, within the expected noise from genes with no knockout phenotype (see Methods). As a result, when we compared cell lines screened by both groups, the Avana data yielded many more TSG hits (**Supplementary Figure 3a**). While most of these do not meet our threshold for PS genes in the Sanger data, hits at our 10% FDR threshold across all Avana screens are strongly biased toward positive Z-scores in the Sanger screens (**Supplementary Figure 3b**), consistent with a weaker signal of positive selection as a result of the shorter assays rather than a lack of robustness in the screens[49].

Discovering Pathways Modulating Cell Growth With A Proliferation Suppressor Co-Occurrence Network

Although known TSG act as PS genes in only a subset of cell lines, we observed patterns of co-occurrence among functionally related genes. *PTEN* co-occurs with mTOR regulators *NF2*[50] ($P < 2x10^{-6}$, Fisher's exact test) and the *TSC1*/*TSC2* complex (P-values both $< 2x10^{-13}$)[51], as well as Programmed Cell Death 10 (*PDCD10*)[52], a proposed tumor suppressor[8,53] (**Figure 2a**). The p53 regulatory cluster (*TP53*, *CDKN1A*, *CHECK2*, *TP53BP1*) also exhibited a strong co-occurrence pattern that was independent of the mTOR regulatory cluster (**Figure 2a**). mTOR[54] and cell cycle checkpoint genes[55,56] have been heavily linked to cancer development, given their roles in controlling cell growth and proliferation, and thus have been the focus of studies characterizing patient genomic profiles to identify common pathway alterations[57,58].

The modularity of mTOR regulators and TP53 regulators demonstrates pathway-level proliferation suppressor activity. This reflects the concept of genes with correlated fitness profiles indicating the genes operate in the same biochemical pathway or biological process[19,21,59,60]. However, the sparseness of PS genes, coupled with their smaller effect sizes,

renders correlation networks relatively poor at identifying modules of genes with proliferation suppressor activity. In order to identify such modules, we developed a PS network based on statistical overrepresentation of co-occurring PS genes (**Figure 2b**); see Methods for details. This approach yields a network of 103 genes containing 157 edges in disconnected clusters; only 9 clusters have 3 or more genes (**Figure 2c** and **Supplementary Figure 4c**). Of these 157 edges, 31 (20.1%, empirical $P<10^{-4}$) are present in the HumanNet[61] functional interaction network (**Supplementary Figure 4a-b**), indicating high functional coherence between connected genes. The network recovers the PTEN and TP53 modules as well as the Hippo pathway, the aryl hydrocarbon receptor complex (AHR/ARNT), the mTOR-repressing GATOR1 complex, the STAGA chromatin remodeling complex, TYK2-STAT signaling, and the gamma-secretase complex (**Figure 2c**), all of which have been associated with tumor suppressor activity. The functional coherence and biological relevance of the PS co-occurrence network further validates the approach taken, and establishes this dataset as a resource for exploring putative tumor suppressor activity in cell lines and tumors.

Variation in Fatty Acid Metabolism in AML Cells

In addition to the known tumor suppressors, we observed a large module containing elements of several fatty acid (FA) and lipid biosynthesis pathways (**Figure 2c**). Interestingly, while there does not appear to be a strong tissue specificity signature for most clusters (**Figure 2c**), the fatty acid metabolism cluster shows a strong enrichment for AML cell lines ($P = 1.1x10^{-5}$). AML, like most cancers, typically relies on increased glucose consumption for energy and diversion of glycolytic intermediates for the generation of biomass required for cell proliferation. Membrane biomass is generated by phospholipid biosynthesis that uses fatty acids as building blocks, with FA pools replenished by some combination of triglyceride catabolism, transporter-mediated uptake, and *de novo* synthesis via the *ACLY/ACACA/FASN* palmitate production pathway using citrate precursor diverted from the TCA cycle. Indeed the role of lipid metabolism in AML progression is indicated by changes in serum lipid content[62] in particular for long-chain saturated fatty acids that are the terminal product of the FAS pipeline. Inhibition of FA synthesis is therefore an appealing chemotherapeutic intervention[63,64] and FASN inhibitors are currently undergoing clinical trials for treatment of solid tumors and metabolic diseases[40]. The observation that knocking out FAS pathway genes results in *faster* proliferation in some AML cells, and their signature as putative tumor suppressor genes, is therefore very unexpected, and in our view warrants further study.

To learn whether additional elements of lipid metabolism were associated with the FAS cluster, we examined the differential correlation of shuffled Z-scores in AML cells. We and others have shown that genes with correlated gene knockout fitness profiles in CRISPR screens are likely to be involved in the same biological pathway or process ("co-functional")[18–21] , analogous to correlated genetic interaction profiles in yeast [25,27,65]. Strikingly, all gene pairs within the fully connected clique in the FAS cluster (containing genes *FASN*, *ACACA*, *GPAT4*, *CHP1*, and *GPI,* **Figure 2c**) had a median Pearson correlation coefficient (PCC) of 0.90 in the 15 AML cell lines (range 0.87-0.97, **Figure 3a**, red), compared to median correlation of 0.18 in the remaining 548 cell lines (range -0.04-0.58, with the highest correlation between *FASN* and *ACACA*, adjacent enzymes in the linear palmitate synthesis pathway; **Figure 3a,** gray). These high differential Pearson correlation coefficients (dPCC) suggest that variation in lipid metabolism is pronounced in AML cells[66].

We sought to explore whether this difference in correlation identified other genes that might give insight into metabolic rewiring in AML. Calculating a global difference between PCC of all gene pairs in AML and in the remaining >500 cell lines yielded many gene pairs whose dPCC appeared indistinguishable from random sampling (**Supplementary Figure 5a-b**). To filter these, we calculated empirical P-values for each gene pair. We randomly selected 15 cell lines from the pool of all screens, calculated PCC for all gene pairs in the selected and remaining lines, and calculated dPCC from these PCC values (**Figure 3b**). We repeated this process 1,000 times to generate an empirically-derived null distribution of dPCC values for each gene pair, against which a P-value could be computed (**Figure 3c-d**).

Expanding the set to a filtered list of genes whose correlation with a gene in the FAS clique showed significant change in AML cells ($P<0.001$; see Methods) yielded a total of 61 genes, including the 5 genes in the clique (**Figure 3e**) and the remaining genes in the co-occurrence network cluster (*LSS, ERO1A, SLC2A1, PGP*) plus Holocarboxylase Synthetase (*HLCS*), which biotinylates and activates acetyl-CoA-carboxylase, the protein product of *ACACA*. Interestingly, about a third of the genes showed significantly increased anticorrelation with the FAS cluster, indicating genes preferentially essential where the FAS genes act as proliferation suppressors (**Figure 3e**). These genes include fatty acid desaturase (*SCD*), which operates directly downstream from FASN to generate monounsaturated fatty acid species, and Sterol Regulatory Element Binding Transcription Factor 1 (*SREBF1*), the master regulatory factor for lipid

homeostasis in cells. Other lipid pathways are also represented, including plasmanylethanolamine desaturase (*TMEM189*), critical for plasmalogen synthesis[67], and ceramide synthase 2 (*CERS2*), involved in *de novo* ceramide biosynthesis[68], an important precursor for sphingomyelin in cell membranes.

Clustering the AML cells lines according to these high dPCC genes reveals two distinct subsets of cells. The FAS cluster and its correlates show strong proliferation suppressor phenotype in four cell lines, NB4, MV411, MOLM13, and THP1. The remaining eleven AML cell lines show negligible to weakly essential phenotypes when these genes are knocked out. The anticorrelated genes, including *SCD* and *SREBF1*, show heightened essentiality in these same cell lines. Together these observed shifts in gene knockout fitness indicates that this subset of AML cells has a specific metabolic rewiring. Because these cells share a genetic signature among fatty acid synthesis pathway genes that is consistent with tumor suppressors, we call these cell lines Fatty Acid Synthesis/Tumor Suppressor (FASTS) cells (**Figure 3e**).

Cas12a-mediated Genetic Interaction Screens Confirm Rewired Lipid Metabolism

We sought to confirm whether gene knockout confers improved cell fitness, and to gather some insight into why some AML cells show the FASTS phenotype and others do not. We designed a CRISPR screen that measures the genetic interactions between eight selected “query genes” and ~100 other genes (“array genes”). The query genes include *FASN* and *ACACA*, from the cluster of proliferation-suppressor genes, as well as lipid homeostasis transcription factor *SREBF1*, anticorrelated with the FAS cluster in the differential network analysis, and uncharacterized gene *c12orf49*, previously implicated in lipid metabolism by coessentiality[21] and a recent genetic interaction study[60]. Additional query genes include control tumor suppressor genes *TP53* and *PTEN* and control context-dependent essential genes *GPX4* and *PSTK* (**Figure 4a**). The array genes include two to three genes each from several metabolic pathways, including various branches of lipid biosynthesis, glycolysis and glutaminolysis, oxphos, peroxisomal and mitochondrial fatty acid oxidation. We include the query genes in the array gene set (**Figure 4a**) to test for screen artifacts and further add control essential and nonessential genes to measure overall screen efficacy (**Supplementary Table 3-4**).

We used the enCas12a CRISPR endonuclease system to carry out multiplex gene knockouts[35] . We used a dual-guide enCas12a design, as described in DeWeirdt *et al.*[34], that allows for

construction of specific guide pairs through pooled oligonucleotide synthesis (**Figure 4b**). The library robustly measures single knockout fitness by pairing three Cas12a crRNA per target gene each with five crRNA targeting nonessential genes[8,43] (n=15 constructs for single knockout fitness), and efficiently assays double knockout fitness by measuring all guides targeting query-array gene pairs (n=9) (**Figure 4c & Supplementary Table 4**). Using this efficient design and the endogenous multiplexing capability of enCas12a, we were able to synthesize a library targeting 800 gene pairs with a single 12k oligonucleotide array.

We screened one AML cell line from the FASTS subset, MOLM13, and a second one with no FAS phenotype, NOMO1, collecting samples at 14 and 21 days after transduction with a five-day puromycin selection (**Supplementary Table 5-6**). Importantly, by comparing the mean log fold change of query gene knockouts in the "A" position *vs.* the same genes in the "B" position of the dual knockout vector, we find no positional bias in the multiplex knockout constructs (**Figure 4d**), consistent with our previous findings[23,34]. Single knockout fitness measurements effectively segregated known essential genes from nonessentials, confirming the efficacy of the primary screens (**Supplementary Figure 6**). Context-dependent fitness profiles are consistent with the cell genotypes, with *PTEN* and *TSC1* showing positive selection in $PTEN^{wt}$ NOMO1 cells and *TP53* being a strong PS gene in $P53^{wt}$ MOLM13 cells. Strikingly, *CHP1* and *GPAT4* are the next two top hits in MOLM13, confirming their proliferation suppressor phenotype (**Figure 4e**), while neither shows a phenotype in NOMO1. Together these observations validate the enCas12a-mediated multiplex perturbation platform, confirm the ability of CRISPR knockout screens to detect proliferation suppressors, and corroborate the background-specific fitness enhancing effects of genes from the FAS cluster.

To measure genetic interactions, we fit a linear regression for each guide between the combination LFCs and the single guide LFCs, Z-scoring the residuals from this line, and combining across all guides targeting the same gene pair (**Supplementary Figure 6 & Supplementary Table 6**). Here, positive genetic interaction Z-scores reflect greater fitness than expected and negative Z-scores represent lower than expected based on the single gene knockouts independently, similar to the methodology applied in a recent survey of genetic interactions in cancer cells using multiplex CRISPR perturbation[33] (see Methods). Gene self-interactions (when the same gene is in the A and B position, **Figure 4d**) should therefore be negative for proliferation suppressors and positive for essentials (**Figure 4f-g**, **Supplementary Figure 6**). Overall, genetic interaction Z-scores in the two cell lines showed moderate

correlation (**Figure 4g**) and previously reported synthetic interactions between *C12orf49* and low-density lipoprotein receptor *LDLR*[17] and between *SREBF1* and its paralog *SREBF2*[17] are identified in both cell lines (**Supplementary Figure 6f-g**).

In contrast with the interactions found in both cell lines, background-specific genetic interactions reflect the genotypic and phenotypic differences between the cells. The negative interaction between tumor suppressor *PTEN* and mTOR repressor *TSC1* in *PTEN*^{wt} NOMO1 cells is consistent with their epistatic roles in the mTOR regulatory pathway. Both genes show positive knockout fitness in NOMO1 (**Figure 4e**) but their dual knockout does not provide an additive growth effect, resulting in a suppressor interaction with a negative Z-score (**Figure 4g-h**). Similarly, suppressor genetic interactions between *ACACA* and downstream proliferation suppressor genes *CHP1* and *GPAT4* are pronounced in MOLM13 cells, consistent with epistatic relationships in a linear biochemical pathway (**Figure 4h**). These interactions are not replicated with query gene *FASN*, but both *FASN* and *ACACA* show negative interactions with fatty acid transport gene *FABP5* and positive interactions with *SREBF1* and *SCD,* the primary desaturase of long-chain saturated fatty acids. All of these interactions are absent in NOMO1, demonstrating the rewiring of the lipid biosynthesis genetic interaction network between these two cell types (**Figure 4h**).

FASTS Signature Predicts Sensitivity to Saturated Fatty Acids

The significant differences in the single- and double-knockout fitness signatures between the two cell lines suggests a major rewiring of lipid metabolism in these cells. *CHP1* and *GPAT4* are reciprocal top correlates in the Avana coessentiality network (r=0.43, P=2.5x10^{-34}), strongly predicting gene co-functionality[21]. Two recent studies characterized the role of lysophosphatidic acid acyltransferase *GPAT4* in adding saturated acyl moieties to glycerol 3-phosphate, generating lysophosphatidic acid (LPA) and phosphatidic acid (PA), the precursors for cellular phospholipids and triglycerides, and further discovered *CHP1* as a key regulatory factor for *GPAT4* activity[69,70]. Within hematological cancer cell lines, the coessentiality network is significantly restructured, with the *ACACA*/*FASN* module correlated with *SCD* in most backgrounds (r=0.33) but strongly anticorrelated (r=-0.63) in blood cancers (**Figure 3e**). The magnitude of this change in correlation is ranked #7 out of 164 million gene pairs, with the other six comprising interactions that are specific to other contexts -- e.g. *BRAF-SOX10* are anticorrelated in blood (r= -0.41) but highly correlated ex-blood (r=0.59) due to their co-

essentiality in *BRAF*^{V600E} melanoma cells. In contrast, *ACACA* and *FASN* are weakly correlated with *CHP1* in most tissues but strongly correlated in AML, with underlying covariation largely driven by the PS phenotype in FASTS cells (**Figure 3e**). This pathway sign reversal is confirmed in the single knockout fitness observed in our screens: *SCD* is strongly essential in MOLM-13 but not in NOMO-1 (**Figure 4e**).

Collectively these observations make a strong prediction about the metabolic processing of specific lipid species. Faster proliferation upon knockout of genes related to saturated fatty acid processing, coupled with increased dependency on fatty acid desaturase (**Figure 5a**), suggests that these cells are at or near their carrying capacity for saturated fatty acids. To test this prediction, we exposed three FASTS cell lines and four other AML cell lines to various species of saturated and unsaturated fatty acids. FASTS cells showed significantly increased apoptosis in the presence of 200 µm palmitate (**Figure 5b-c**) while no other species of saturated or unsaturated fatty acid showed similar differential sensitivity. In addition, analysis of metabolic profiles of cells in the Cancer Cell Line Encyclopedia[71,72] showed that saturated acyl chains are markedly overrepresented in triacylglycerol (TAG) in FASTS cells (**Figure 5d**), in contrast with other lipid species measured **(Supplementary Figure 7**). Palmitate-induced lipotoxicity has been studied in many contexts – and importantly, the role of *GPAT4* and *CHP1* in mediating lipotoxicity was well described recently[69,70] – but, to our knowledge, this is the first instance of a genetic signature that predicts liposensitivity.

Clinical Relevance of FASTS Subtype

To explore whether the FASTS phenotype has clinical relevance, we compared our results with patient survival information from public databases. Using genetic characterization data from CCLE[71], we did not find any lesion which segregated FASTS cells from other CD33+ AML cells (**Figure 6a**), so no mutation is nominated to drive a FASTS phenotype *in vivo*. Instead, we explored whether variation in gene expression was associated with patient outcomes. We included genes in the core FASTS module as well as genes with strong genetic interactions with *ACACA/FASN* in our screen (**Figure 6a**). To select an appropriate cohort for genomic analysis, we first considered patient age. Although AML is present across every decade of life, patients from whom FASTS cell lines were derived are all under 30 years of age (sources of other AML cells ranged from 7 to 68 years; **Figure 6b**). With this in mind, we explored data from the TARGET-AML[73] project, which focuses on childhood cancers (**Figure 6c**). Using TARGET

data, we calculated hazard ratios using univariate Cox proportional-hazards modeling with continuous mRNA expression values for our genes of interest as independent variables. We observed that both *CHP1* and *GPAT4* show significant, negative hazard ratios (HR), consistent with a tumor suppressor signature (**Figure 6d**), and that no other gene from our set shows a negative HR. Indeed, tumors in the top quartile of gene expression showed significantly improved survival for both *CHP1* (P-value 0.007, **Figure 6e**) and *GPAT4* (P-value 0.035, **Figure 6f**). These findings are not replicated for *CHP1* and *GPAT4* in the TCGA[74] or OHSU[75] tumor genomics data sets, suggesting the FASTS phenotype might be restricted to juvenile leukemias.

Discussion

CRISPR screens have had a profound impact on cancer functional genomics. While research has been mainly focused on essential gene phenotypes, there is still much clinically relevant biology that can be uncovered by examining other phenotypes from a genetic screen. We establish a methodology that can identify the proliferation suppressor phenotype from whole-genome CRISPR knockout genetic screens. This represents, to our knowledge, the first systematic study of this phenotype in the ~1,000 published screens[7,10,11,13,44].

The activity of PS genes is inherently context-dependent, rendering global classification difficult. As with context-dependent essential genes, the strongest signal is attained when comparing knockout phenotype with underlying mutation state. For example, wildtype and mutant alleles of classic tumor suppressor examples *TP53* and *PTEN* are present in large numbers of cell lines, enabling relatively easy discrimination of PS behavior in wildtype backgrounds, but most mutations are much more rare, reducing statistical power. Our model-based approach enables the discovery of PS phenotype as an outlier from null-phenotype knockouts. Using this approach, we recover COSMIC-annotated TSGs exhibiting the PS phenotype when wildtype alleles are expressed at nominal levels.

Co-occurrence of proliferation suppressors follows the principles of modular biology, with genes in the same pathway acting as proliferation suppressors in the same cell lines. We observe background-specific putative tumor suppressor activity for the PTEN pathway, P53 regulation, mTOR signaling, chromatin remodeling, and others. The co-occurrence network also reveals a novel module associated with glycerolipid biosynthesis, which exhibits the PS phenotype in a subset of AML cells. Analysis of the rewiring of the lipid metabolism coessentiality network in

AML cells corroborated this discovery, and led us to define the Fatty Acid Synthesis/Tumor Suppressor (FASTS) phenotype in four AML cell lines. A survey of genetic interactions, using the enCas12a multiplex knockout platform, showed major network rewiring between FASTS and other AML cells, and revealed strong genetic interactions in FASTS cells with *GPAT4*, a key enzyme in the processing of saturated fatty acids, and its regulator *CHP1*. Collectively these observations suggest that FASTS cells are near some critical threshold for saturated fatty acid carrying capacity, which we validated biochemically by treatment with fatty acids and bioinformatically by comparison with CCLE metabolomic profiling.

Confirming the clinical relevance of an *in vitro* phenotype can be difficult. No obvious mutation segregates FASTS cells from other AML cells, and with only four cell lines showing the FASTS phenotype, we lack the statistical power to discover associations in an unbiased way. However, by narrowing our search to strong hits from the differential network analyses, we found a significant survival advantage in a roughly age-matched cohort for *GPAT4* and *CHP1* overexpression. This finding is consistent with a wholly novel tumor suppressor signature for our PS gene module.

The combination of genetic, biochemical, and clinical support for the discovery of a novel tumor suppressor module has several implications. First, it provides a clinical signature that warrants further research as a prognostic marker as well as a potential therapeutic target -- and a high-risk group for fatty acid synthesis inhibitors. Second, it demonstrates the power of differential network analysis, and in particular differential genetic interaction networks, to dissect the rewiring of molecular pathways from modular phenotypes. And finally, it suggests that there still may be much to learn from data-driven analyses of large-scale screen data, beyond the low-hanging fruit of lesion/vulnerability associations.

Acknowledgments

WFL, MMc, MMo, and TH were supported by NIGMS grant R35GM130119. MC is supported by a Kopchick fellowship and Pauline Altman-Goldstein Foundation Discovery Fellowship. EK is supported by a grant from the Prostate Cancer Foundation. MD is supported by a Schissler Foundation fellowship. TH is a CPRIT Scholar in Cancer Research (RR160032). WFL is supported by the American Legion Auxiliary Fellowship in Cancer Research. This work was supported by the Andrew Sabin Family Foundation Fellowship. Flow cytometry was performed at MDACC's Advanced Cytometry & Sorting Facility supported by the NCI Cancer Center Support Grant P30CA16672.

Author Contributions

WFL performed all PS discovery analysis. MF, AG, AS performed genetic interaction screens and PD, MC performed bioinformatic analysis. WFL, MC, EK, and MD performed all other bioinformatic analysis. MMo and MMc performed lipid profiling experiments. JGD and TH supervised the research. WFL and TH drafted the manuscript and all authors edited it.

Competing Interests

TH is a consultant for Repare Therapeutics. JGD consults for Agios, Maze Therapeutics, Microsoft Research, and Pfizer; JGD consults for and has equity in Tango Therapeutics. WFL is a consultant for BioAge Labs.

References

1. Jinek, M. *et al.* A Programmable Dual-RNA–Guided DNA Endonuclease in Adaptive Bacterial Immunity. *Science* **337**, 816–821 (2012).
2. Mali, P. *et al.* RNA-Guided Human Genome Engineering via Cas9. *Science* **339**, 823–826 (2013).
3. Mali, P., Esvelt, K. M. & Church, G. M. Cas9 as a versatile tool for engineering biology. *Nat. Methods* **10**, 957–963 (2013).
4. Cong, L. *et al.* Multiplex genome engineering using CRISPR/Cas systems. *Science* **339**, 819–823 (2013).
5. Shalem, O., Sanjana, N. E. & Zhang, F. High-throughput functional genomics using CRISPR-Cas9. *Nat. Rev. Genet.* **16**, 299–311 (2015).
6. Wang, T., Wei, J. J., Sabatini, D. M. & Lander, E. S. Genetic screens in human cells using the CRISPR-Cas9 system. *Science* **343**, 80–84 (2014).
7. Wang, T. *et al.* Identification and characterization of essential genes in the human genome. *Science* **350**, 1096–1101 (2015).
8. Hart, T. *et al.* High-Resolution CRISPR Screens Reveal Fitness Genes and Genotype-Specific Cancer Liabilities. *Cell* **163**, 1515–1526 (2015).
9. Aguirre, A. J. *et al.* Genomic Copy Number Dictates a Gene-Independent Cell Response to CRISPR/Cas9 Targeting. *Cancer Discov.* **6**, 914–929 (2016).
10. Meyers, R. M. *et al.* Computational correction of copy number effect improves specificity of CRISPR-Cas9 essentiality screens in cancer cells. *Nat. Genet.* **49**, 1779–1784 (2017).
11. Tsherniak, A. *et al.* Defining a Cancer Dependency Map. *Cell* **170**, 564-576.e16 (2017).
12. Tzelepis, K. *et al.* A CRISPR Dropout Screen Identifies Genetic Vulnerabilities and Therapeutic Targets in Acute Myeloid Leukemia. *Cell Rep.* **17**, 1193–1205 (2016).
13. Behan, F. M. *et al.* Prioritization of cancer therapeutic targets using CRISPR-Cas9 screens.

Nature **568**, 511–516 (2019).

14. Lagziel, S., Lee, W. D. & Shlomi, T. Inferring cancer dependencies on metabolic genes from large-scale genetic screens. *BMC Biol.* **17**, 37 (2019).
15. Rossiter, N. J. *et al.* CRISPR screens in physiologic medium reveal conditionally essential genes in human cells. *bioRxiv* 2020.08.31.275107 (2020) doi:10.1101/2020.08.31.275107.
16. Zhao, D. *et al.* Combinatorial CRISPR-Cas9 Metabolic Screens Reveal Critical Redox Control Points Dependent on the KEAP1-NRF2 Regulatory Axis. *Mol. Cell* **69**, 699-708.e7 (2018).
17. Aregger, M. *et al.* Systematic mapping of genetic interactions for de novo fatty acid synthesis identifies C12orf49 as a regulator of lipid metabolism. *Nat. Metab.* **2**, 499–513 (2020).
18. Wang, T. *et al.* Gene Essentiality Profiling Reveals Gene Networks and Synthetic Lethal Interactions with Oncogenic Ras. *Cell* **168**, 890-903.e15 (2017).
19. Boyle, E. A., Pritchard, J. K. & Greenleaf, W. J. High-resolution mapping of cancer cell networks using co-functional interactions. *Mol. Syst. Biol.* **14**, e8594 (2018).
20. Rauscher, B. *et al.* Toward an integrated map of genetic interactions in cancer cells. *Mol. Syst. Biol.* **14**, e7656 (2018).
21. Kim, E. *et al.* A network of human functional gene interactions from knockout fitness screens in cancer cells. *Life Sci. Alliance* **2**, (2019).
22. Kegel, B. D. & Ryan, C. J. Paralog buffering contributes to the variable essentiality of genes in cancer cell lines. *PLOS Genet.* **15**, e1008466 (2019).
23. Dede, M., McLaughlin, M., Kim, E. & Hart, T. Multiplex enCas12a screens show functional buffering by paralogs is systematically absent from genome-wide CRISPR/Cas9 knockout screens. *bioRxiv* 2020.05.18.102764 (2020) doi:10.1101/2020.05.18.102764.
24. Beltrao, P., Cagney, G. & Krogan, N. J. Quantitative genetic interactions reveal biological modularity. *Cell* **141**, 739–745 (2010).

25. Costanzo, M. *et al.* The genetic landscape of a cell. *Science* **327**, 425–431 (2010).
26. Martin, H. *et al.* Differential genetic interactions of yeast stress response MAPK pathways. *Mol. Syst. Biol.* **11**, 800 (2015).
27. Costanzo, M. *et al.* A global genetic interaction network maps a wiring diagram of cellular function. *Science* **353**, (2016).
28. Wong, A. S. L. *et al.* Multiplexed barcoded CRISPR-Cas9 screening enabled by CombiGEM. *Proc. Natl. Acad. Sci.* **113**, 2544–2549 (2016).
29. Shen, J. P. *et al.* Combinatorial CRISPR–Cas9 screens for de novo mapping of genetic interactions. *Nat. Methods* **14**, 573–576 (2017).
30. Han, K. *et al.* Synergistic drug combinations for cancer identified in a CRISPR screen for pairwise genetic interactions. *Nat. Biotechnol.* **35**, 463–474 (2017).
31. Najm, F. J. *et al.* Orthologous CRISPR-Cas9 enzymes for combinatorial genetic screens. *Nat. Biotechnol.* **36**, 179–189 (2018).
32. Du, D. *et al.* Genetic interaction mapping in mammalian cells using CRISPR interference. *Nat. Methods* **14**, 577–580 (2017).
33. Horlbeck, M. A. *et al.* Mapping the Genetic Landscape of Human Cells. *Cell* **174**, 953-967.e22 (2018).
34. DeWeirdt, P. C. *et al.* Optimization of AsCas12a for combinatorial genetic screens in human cells. *Nat. Biotechnol.* 1–11 (2020) doi:10.1038/s41587-020-0600-6.
35. Kleinstiver, B. P. *et al.* Engineered CRISPR-Cas12a variants with increased activities and improved targeting ranges for gene, epigenetic and base editing. *Nat. Biotechnol.* **37**, 276–282 (2019).
36. Bandyopadhyay, S. *et al.* Rewiring of genetic networks in response to DNA damage. *Science* **330**, 1385–1389 (2010).
37. Ideker, T. & Krogan, N. J. Differential network biology. *Mol. Syst. Biol.* **8**, 565 (2012).
38. Colic, M. *et al.* Identifying chemogenetic interactions from CRISPR screens with drugZ.

Genome Med. **11**, 52 (2019).

39. Menendez, J. A. & Lupu, R. Fatty acid synthase (FASN) as a therapeutic target in breast cancer. *Expert Opin. Ther. Targets* **21**, 1001–1016 (2017).
40. Search of: FASN - List Results - ClinicalTrials.gov. https://clinicaltrials.gov/search?cond=FASN.
41. Sondka, Z. *et al.* The COSMIC Cancer Gene Census: describing genetic dysfunction across all human cancers. *Nat. Rev. Cancer* **18**, 696–705 (2018).
42. Bamford, S. *et al.* The COSMIC (Catalogue of Somatic Mutations in Cancer) database and website. *Br. J. Cancer* **91**, 355–358 (2004).
43. Hart, T., Brown, K. R., Sircoulomb, F., Rottapel, R. & Moffat, J. Measuring error rates in genomic perturbation screens: gold standards for human functional genomics. *Mol. Syst. Biol.* **10**, 733 (2014).
44. Dempster, J. M. *et al.* Extracting Biological Insights from the Project Achilles Genome-Scale CRISPR Screens in Cancer Cell Lines. *bioRxiv* 720243 (2019) doi:10.1101/720243.
45. DepMap, B. DepMap 19Q2 Public. (2019) doi:10.6084/m9.figshare.8061398.v1.
46. Allen, F. *et al.* JACKS: joint analysis of CRISPR/Cas9 knockout screens. *Genome Res.* **29**, 464–471 (2019).
47. Hart, T. & Moffat, J. BAGEL: a computational framework for identifying essential genes from pooled library screens. *BMC Bioinformatics* **17**, 164 (2016).
48. Kim, E. & Hart, T. Improved analysis of CRISPR fitness screens and reduced off-target effects with the BAGEL2 gene essentiality classifier. *bioRxiv* 2020.05.30.125526 (2020) doi:10.1101/2020.05.30.125526.
49. Dempster, J. M. *et al.* Agreement between two large pan-cancer CRISPR-Cas9 gene dependency data sets. *Nat. Commun.* **10**, 5817 (2019).
50. James, M. F. *et al.* NF2/merlin is a novel negative regulator of mTOR complex 1, and activation of mTORC1 is associated with meningioma and schwannoma growth. *Mol. Cell.*

610 *Biol.* **29**, 4250–4261 (2009).

611 51. Huang, J., Dibble, C. C., Matsuzaki, M. & Manning, B. D. The TSC1-TSC2 complex is
612 required for proper activation of mTOR complex 2. *Mol. Cell. Biol.* **28**, 4104–4115 (2008).

613 52. Marchi, S. *et al.* Defective autophagy is a key feature of cerebral cavernous malformations.
614 *EMBO Mol. Med.* **7**, 1403–1417 (2015).

615 53. Zhu, Y. *et al.* Loss of endothelial programmed cell death 10 activates glioblastoma cells and
616 promotes tumor growth. *Neuro-Oncol.* **18**, 538–548 (2016).

617 54. Pópulo, H., Lopes, J. M. & Soares, P. The mTOR signalling pathway in human cancer. *Int.*
618 *J. Mol. Sci.* **13**, 1886–1918 (2012).

619 55. Massagué, J. G1 cell-cycle control and cancer. *Nature* **432**, 298–306 (2004).

620 56. Evan, G. I. & Vousden, K. H. Proliferation, cell cycle and apoptosis in cancer. *Nature* **411**,
621 342–348 (2001).

622 57. Donehower, L. A. *et al.* Integrated Analysis of TP53 Gene and Pathway Alterations in The
623 Cancer Genome Atlas. *Cell Rep.* **28**, 1370-1384.e5 (2019).

624 58. Zhang, Y. *et al.* A Pan-Cancer Proteogenomic Atlas of PI3K/AKT/mTOR Pathway
625 Alterations. *Cancer Cell* **31**, 820-832.e3 (2017).

626 59. Pan, J. *et al.* Interrogation of Mammalian Protein Complex Structure, Function, and
627 Membership Using Genome-Scale Fitness Screens. *Cell Syst.* **6**, 555-568.e7 (2018).

628 60. Bayraktar, E. C. *et al.* Metabolic coessentiality mapping identifies C12orf49 as a regulator of
629 SREBP processing and cholesterol metabolism. *Nat. Metab.* **2**, 487–498 (2020).

630 61. Hwang, S. *et al.* HumanNet v2: human gene networks for disease research. *Nucleic Acids*
631 *Res.* **47**, D573–D580 (2019).

632 62. Khalid, A., Siddiqui, A. J., Huang, J.-H., Shamsi, T. & Musharraf, S. G. Alteration of Serum
633 Free Fatty Acids are Indicators for Progression of Pre-leukaemia Diseases to Leukaemia.
634 *Sci. Rep.* **8**, 14883 (2018).

635 63. Flavin, R., Peluso, S., Nguyen, P. L. & Loda, M. Fatty acid synthase as a potential

therapeutic target in cancer. *Future Oncol.* **6**, 551–562 (2010).

64. Punekar, S. & Cho, D. C. Novel Therapeutics Affecting Metabolic Pathways. *Am. Soc. Clin. Oncol. Educ. Book* e79–e87 (2019) doi:10.1200/EDBK_238499.
65. Roguev, A. *et al.* Conservation and rewiring of functional modules revealed by an epistasis map in fission yeast. *Science* **322**, 405–410 (2008).
66. Li, K.-C. Genome-wide coexpression dynamics: Theory and application. *Proc. Natl. Acad. Sci. U. S. A.* **99**, 16875–16880 (2002).
67. Gallego-García, A. *et al.* A bacterial light response reveals an orphan desaturase for human plasmalogen synthesis. *Science* **366**, 128–132 (2019).
68. Mullen, T. D., Hannun, Y. A. & Obeid, L. M. Ceramide synthases at the centre of sphingolipid metabolism and biology. *Biochem. J.* **441**, 789–802 (2012).
69. Piccolis, M. *et al.* Probing the Global Cellular Responses to Lipotoxicity Caused by Saturated Fatty Acids. *Mol. Cell* **74**, 32-44.e8 (2019).
70. Zhu, X. G. *et al.* CHP1 Regulates Compartmentalized Glycerolipid Synthesis by Activating GPAT4. *Mol. Cell* **74**, 45-58.e7 (2019).
71. Ghandi, M. *et al.* Next-generation characterization of the Cancer Cell Line Encyclopedia. *Nature* **569**, 503–508 (2019).
72. Li, H. *et al.* The landscape of cancer cell line metabolism. *Nat. Med.* **25**, 850–860 (2019).
73. Meshinchi, S. & Arceci, R. TARGET: Acute Myeloid Leukemia (AML), dbGaP Study Accession: phs000465.v19.p8. https://www.ncbi.nlm.nih.gov/projects/gap/cgi-bin/study.cgi?study_id=phs000465.v19.p8.
74. Genomic and Epigenomic Landscapes of Adult De Novo Acute Myeloid Leukemia. *N. Engl. J. Med.* **368**, 2059–2074 (2013).
75. Tyner, J. W. *et al.* Functional genomic landscape of acute myeloid leukaemia. *Nature* **562**, 526–531 (2018).

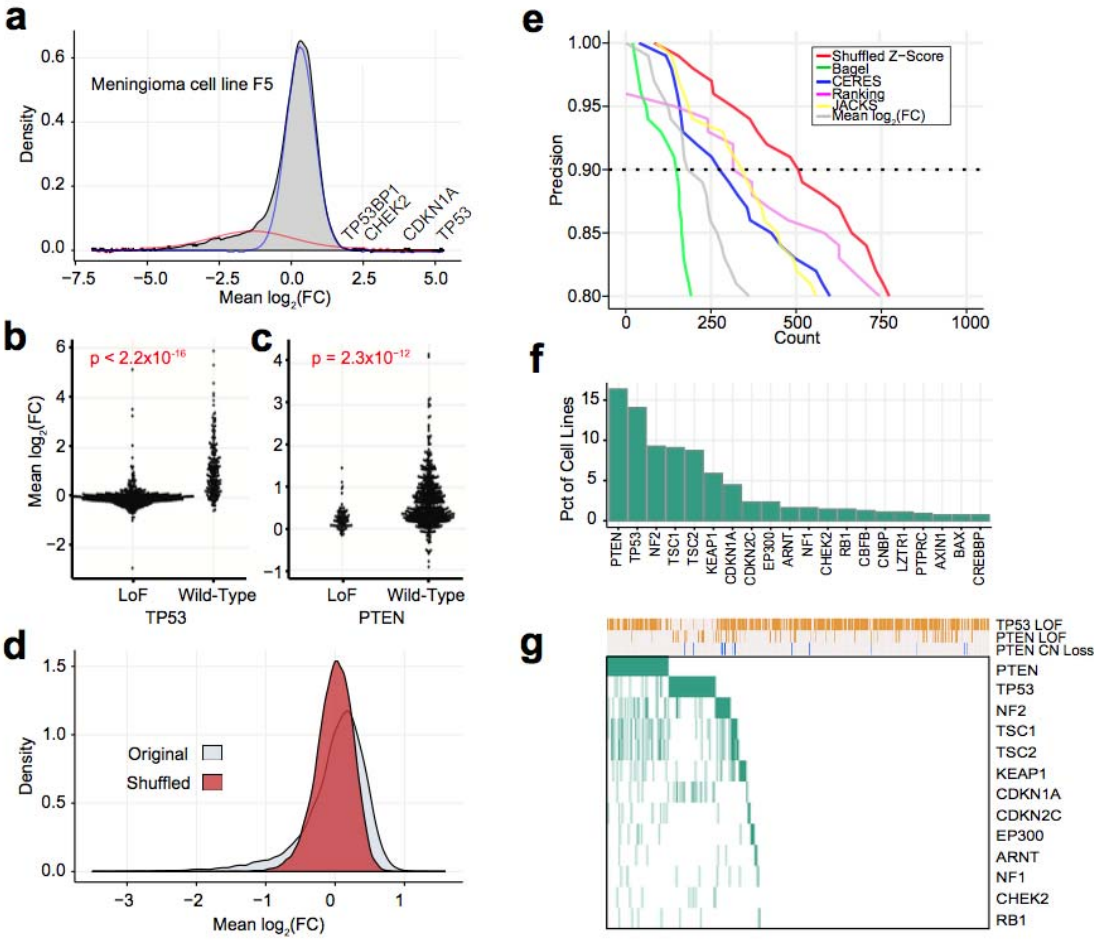

Figure 1. Discovery of Proliferation Suppressor genes. (a) Fold-change distribution of a typical CRISPR knockout screen has a long left tail of essential genes, and a small number of genes whose knockout increases fitness (proliferation suppressors, “PS genes”). (b) and (c) Fold change of known tumor suppressors across 563 cell lines. Red, P-values are from corresponding Wilcoxon rank-sum tests. (d) Distribution of mean log fold change before and after label-shuffling. (e) Precision vs. recall of shuffled Z-score and other CRISPR analysis methods. Dashed line, 90% precision (10% FDR). (f) Fraction of cell lines in which known tumor suppressors are classified as PS genes at 10% FDR. (g) Presence of each known TSG across 563 cell lines, vs. cell genetic background. Gold, mutation present; gray, absent. Green, gene is classified as a proliferation suppressor.

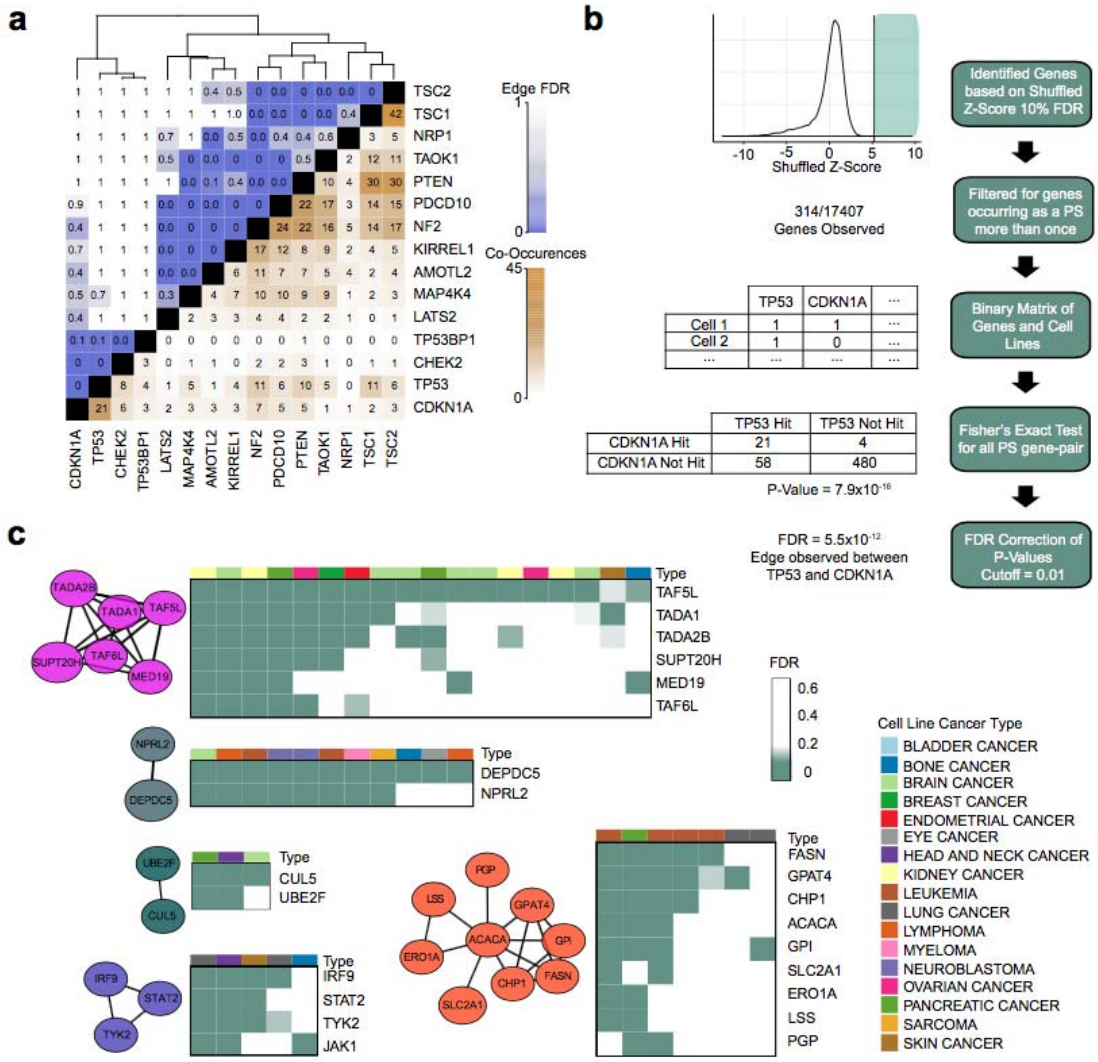

	TP53	CDKN1A	...
Cell 1	1	1	...
Cell 2	1	0	...
...	...	...	...

	TP53 Hit	TP53 Not Hit
CDKN1A Hit	21	4
CDKN1A Not Hit	58	480

Figure 2. Co-occurrence of PS genes. (a) Co-occurrence/mutual exclusivity of common TSG as PS genes in CRISPR screens. Brown, number of cell lines in which two genes co-occur as PS genes at 10% FDR. Blue, FDR of co-occurrence. Hierarchical clustering indicates functional modules. (b) Pipeline for building the co-PS network. (c) Examples from the Co-PS network. Nodes are connected by edges at FDR < 1%. Heatmaps indicate presence of PS gene vs. cell lineage. The fatty acid synthesis cluster (orange) is selected for further analysis.

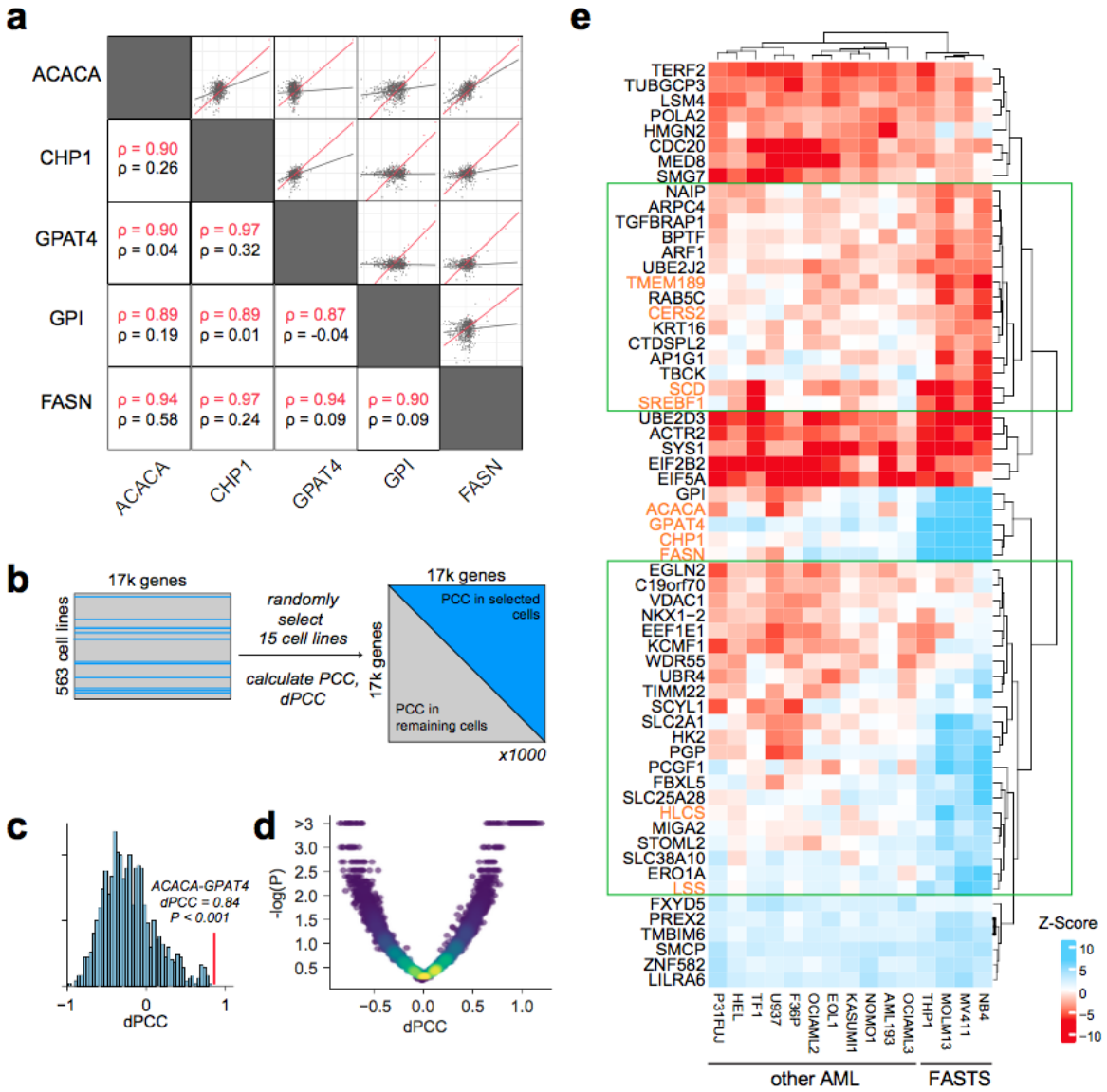

Figure 3. Differential network analysis of fatty acid synthesis module. (a) Among genes in the FAS module, Pearson correlation coefficients of shuffled Z score profiles are substantially higher in AML cells (red) than in other cells (gray). (b) Significance testing of differential PCC (dPCC) involves building a null distribution by randomly selecting 15 cell lines, and calculating PCC between all gene pairs in the selected cells and the remaining cells. (c) After 1,000 repeats, a null distribution is generated for each pair, and a P-value is calculated for the observed AML-vs-other dPCC. (d) Volcano plot of dPCC vs. P-value. (e) Heatmap of shuffled Z score for 15 AML cell lines vs. genes with P<0.001 and |Z| > 3 in at least one AML cell line.

696 Clustering indicates the putative Fatty Acid Synthesis/Tumor Suppressor (FASTS) subtype.
697 Green boxes indicate genes that are preferentially essential (top) or nonessential (bottom) in
698 FASTS. Orange, genes involved in fatty acid and membrane biosynthesis.
699

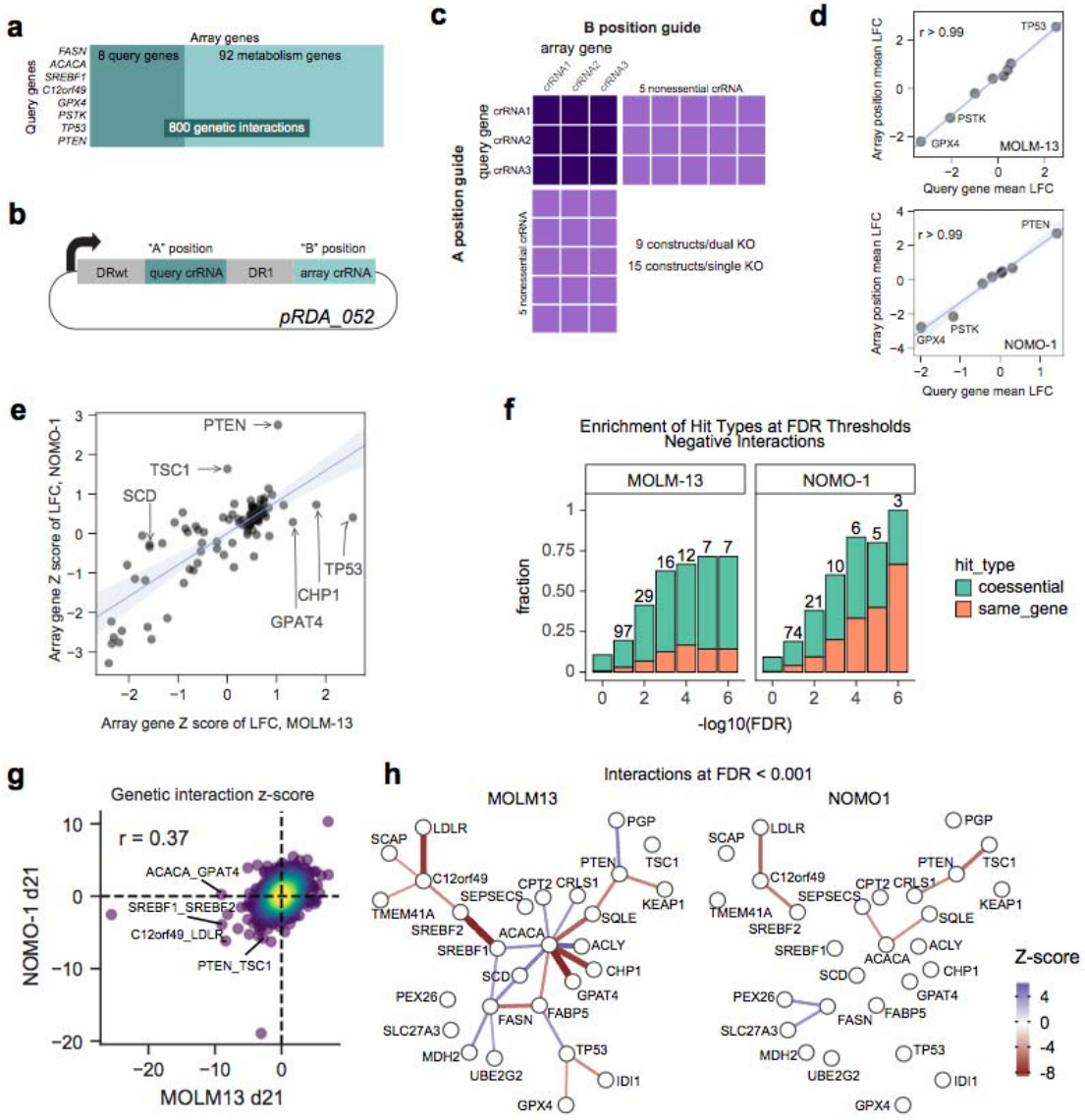

Figure 4. Genetic interactions reveal a rewired lipid biosynthesis pathway in FASTS cells. (a) Genetic interaction screen targets 8 query genes and 100 array genes, for a total of 800 pairwise knockouts. (b) Library design uses a dual-guide enCa12a expression vector which targets the query gene in the "A" position and array gene in the "B" position. (c) Overall library design includes three crRNA/gene plus control crRNA targeting nonessential genes. Single-knockout constructs (target gene paired with nonessential controls) allow accurate measurement of single knockout fitness. (d) Considering single knockout fitness of query genes in the "A" and "B" position of the crRNA expression vector shows no position effects in the two

712 cell lines screened (MOLM-13, NOMO-1). LFC, log fold change. (e) Single knockout fitness (Z-
713 score of mean LFC) is highly consistent between MOLM-13 and NOMO-1, but reveals
714 background-specific PS genes. (f) Enrichment among GI for coessential and same-gene genetic
715 interactions. Same-gene interactions among genes that show single knockout fitness
716 phenotypes are expected, reflecting quality of GI observations. (g) Global comparison of MOLM-
717 13, NOMO-1 genetic interaction Z scores. (h) Network view of interactions in each background
718 shows rewiring in MOLM-13 FASTS cells.
719

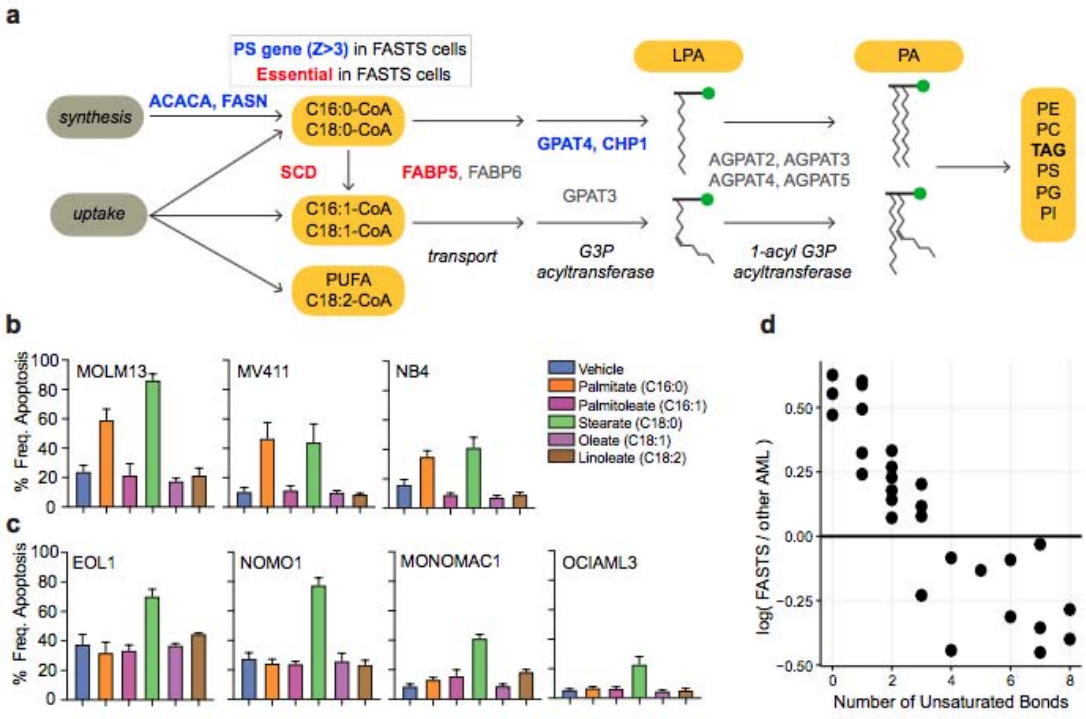

Figure 5. FASTS cells are sensitive to saturated FA. (a) Schematic of the fatty acid/glycerolipid synthesis pathway. Blue, PS genes in FASTS cells. Red, essential genes. Pathway analysis suggests saturated fatty acids are a critical node. (b) Apoptosis of FASTS cells in response to media supplemented with 200 µm fatty acids. All three cell lines show marked sensitivity to palmitate. (c) Apoptosis of other AML cells in response to fatty acids shows no response to palmitate. (d) Triacylglycerol (TAG) species metabolite differences. The x axis represents the median difference of log10 normalized peak area of the metabolite in FASTS cells vs all other AML cells. The y axis represents the number of saturated bonds present. Each dot represents a unique metabolite.

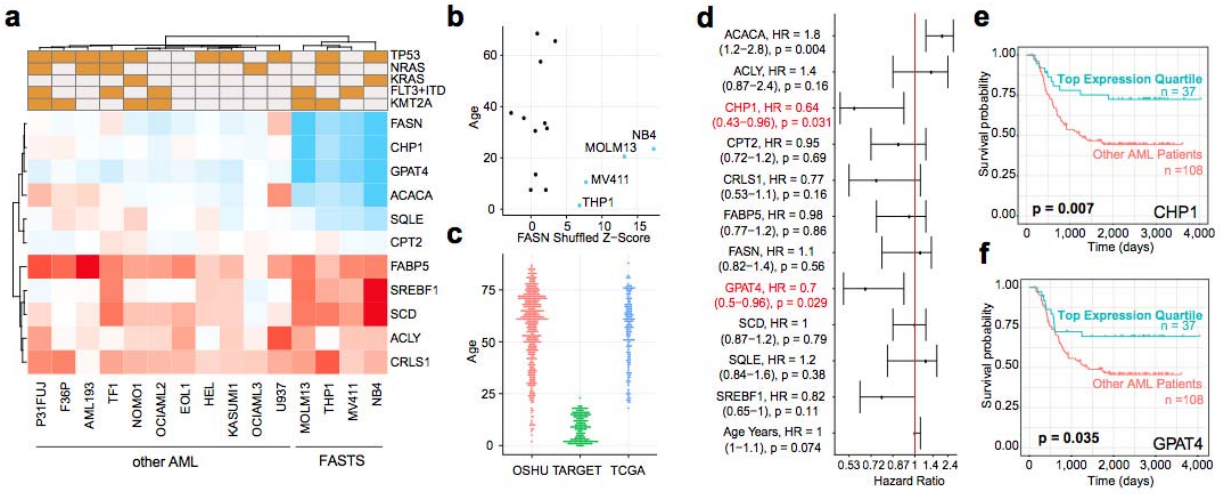

Figure 6. Prognostic signature of FASTS module. (a) Heatmap of shuffled Z scores for genes implicated in the genetic interaction network. Top, common AML lesions. (b) Shuffled Z-score of FASN in AML cell lines vs. age of patient from which cell lines were derived. Blue, FASTS cells. (c) Age distribution of AML patients in three genomics cohorts. (d) Hazard ratios (95% CI; univariate Cox proportional hazards test) for expression of genes in (a), using genomics and survival data from TARGET. (e) Kaplan-Meier survival analysis of AML patients in TARGET, comparing top quartile of *CHP1* expression vs. others. (e) Same, with *GPAT4*.